Supporting Information

GSH-sensitive Pt(IV) prodrug-loaded phase-transitional nanoparticles with a hybrid lipid-polymer shell for precise theranostics against ovarian cancer

Hui Huang, Yang Dong, Yanhua Zhang, Dan Ru, Zhihua Wu, Jiali Zhang, Ming Shen, Yourong Duan* and Ying Sun*

State Key Laboratory of Oncogenes and Related Genes, Shanghai Cancer Institute, Renji Hospital, School of Medicine, Shanghai Jiao Tong University, Shanghai 200032, People's Republic of China.

Corresponding author: yrduan@shsci.org; ysun@shsci.org

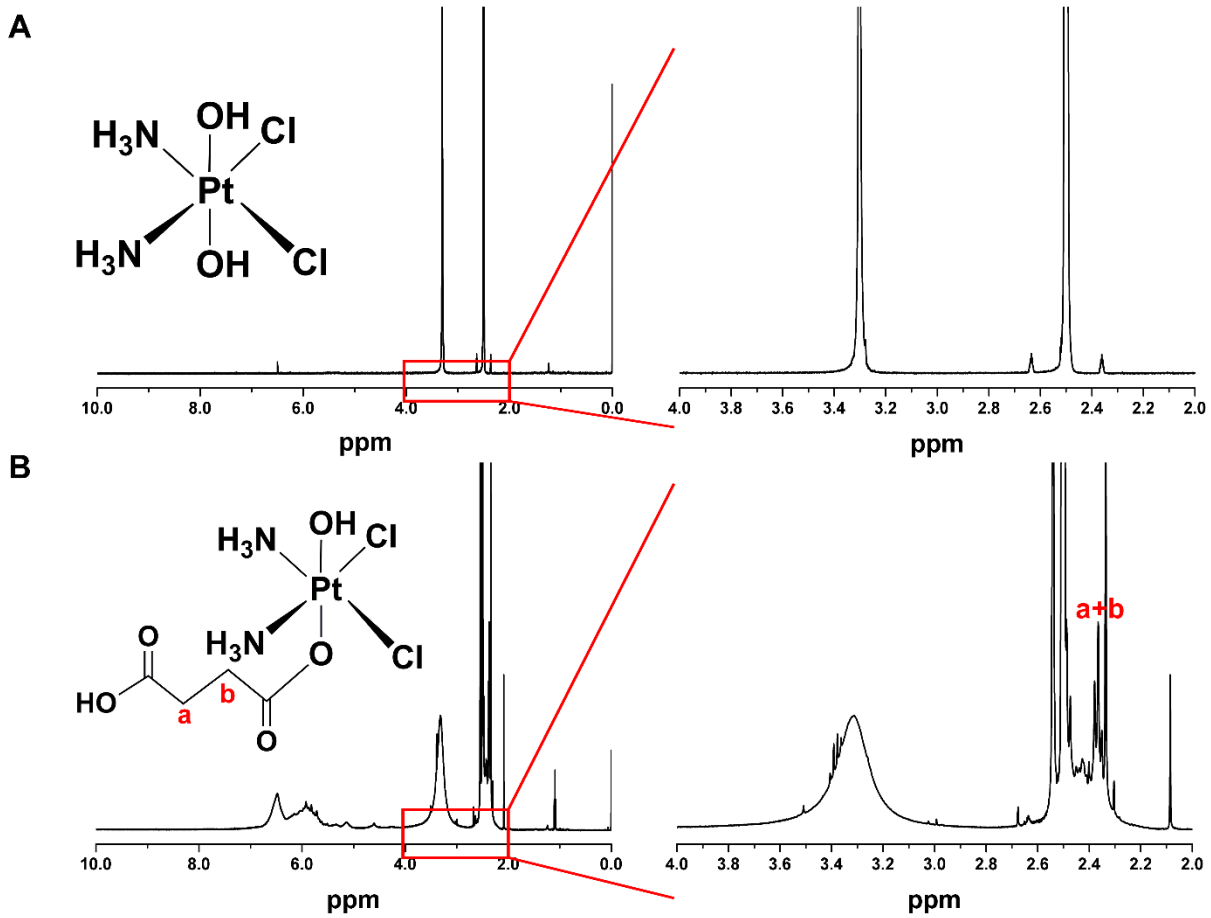

Figure S1. ^{1}H NMR spectra of *c,c,t*-[Pt(NH$_3$)$_2$Cl$_2$(OH)$_2$] **(A)** and *c,c,t*-[Pt(NH$_3$)$_2$Cl$_2$(OOCCH$_2$CH$_2$COOH)(OH)] (Pt(IV)) **(B)** in DMSO-d6. Pt(IV) was isolated in 70.6% (46 mg) yield. ^{1}H NMR (500 MHz, DMSO-d6, ppm): δ 6.0 (br, NH$_3$, 6H), 2.45-2.30 (m, OCCH$_2$CH$_2$CO, 4H).

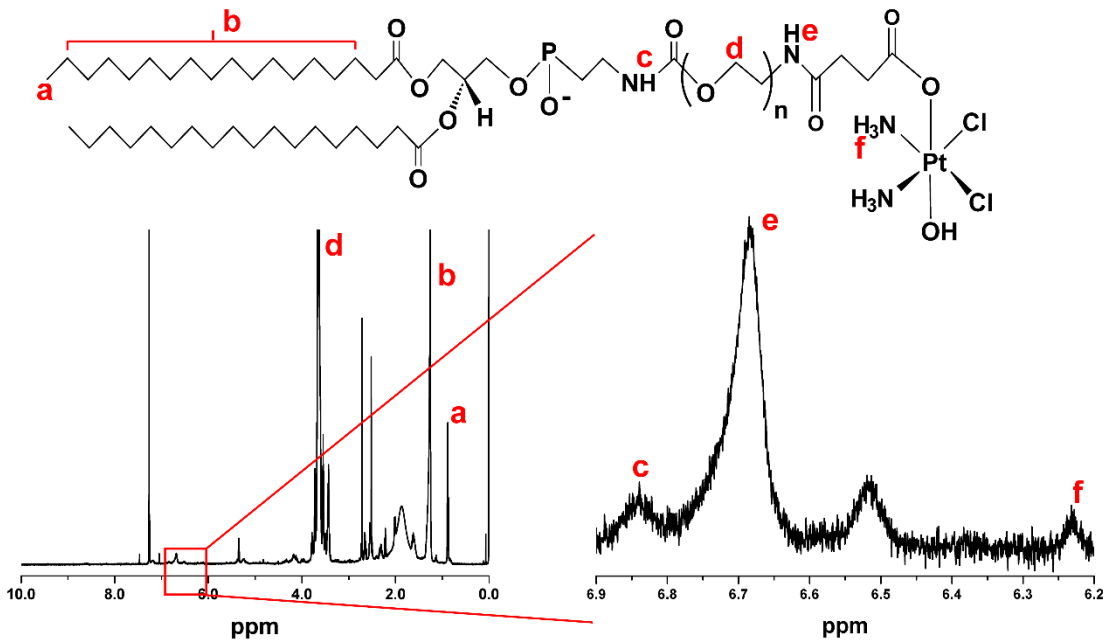

Figure S2. The magnification of ^{1}H NMR spectra of the DSPE-PEG$_{1k}$-Pt(IV) in $CDCl_3$. ^{1}H NMR (500 MHz, $CDCl_3$, ppm): δ 6.23 (bs, NH_3, 6H), 6.68 (bs, $NHCOCH_2$), 6.84 (bs, $NHCOOCH_2$).

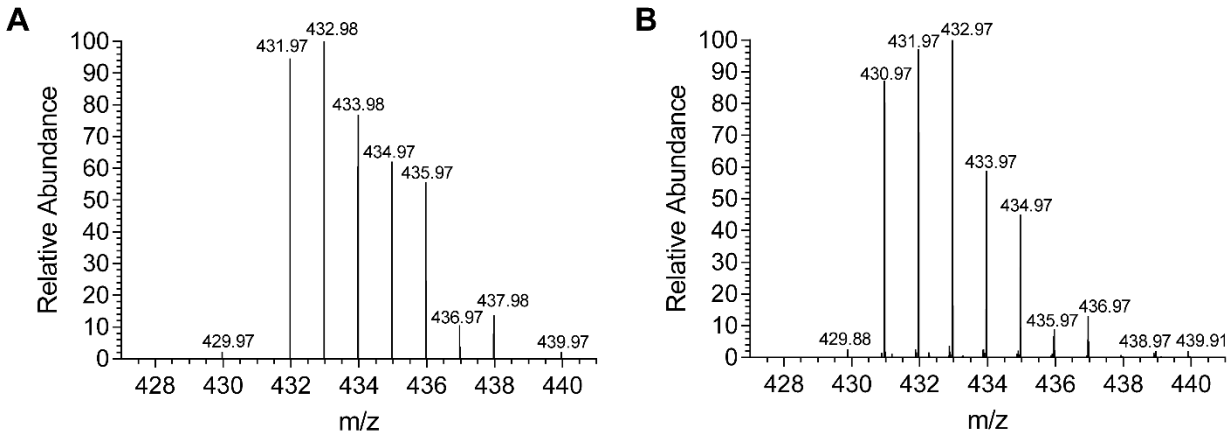

Figure S3. Theoretical isotope pattern **(A)** and experimental results **(B)** of Pt(IV) measured by ESI-MS. ESI-MS (negative mode) Calc. = 434.14, Found = 432.97.

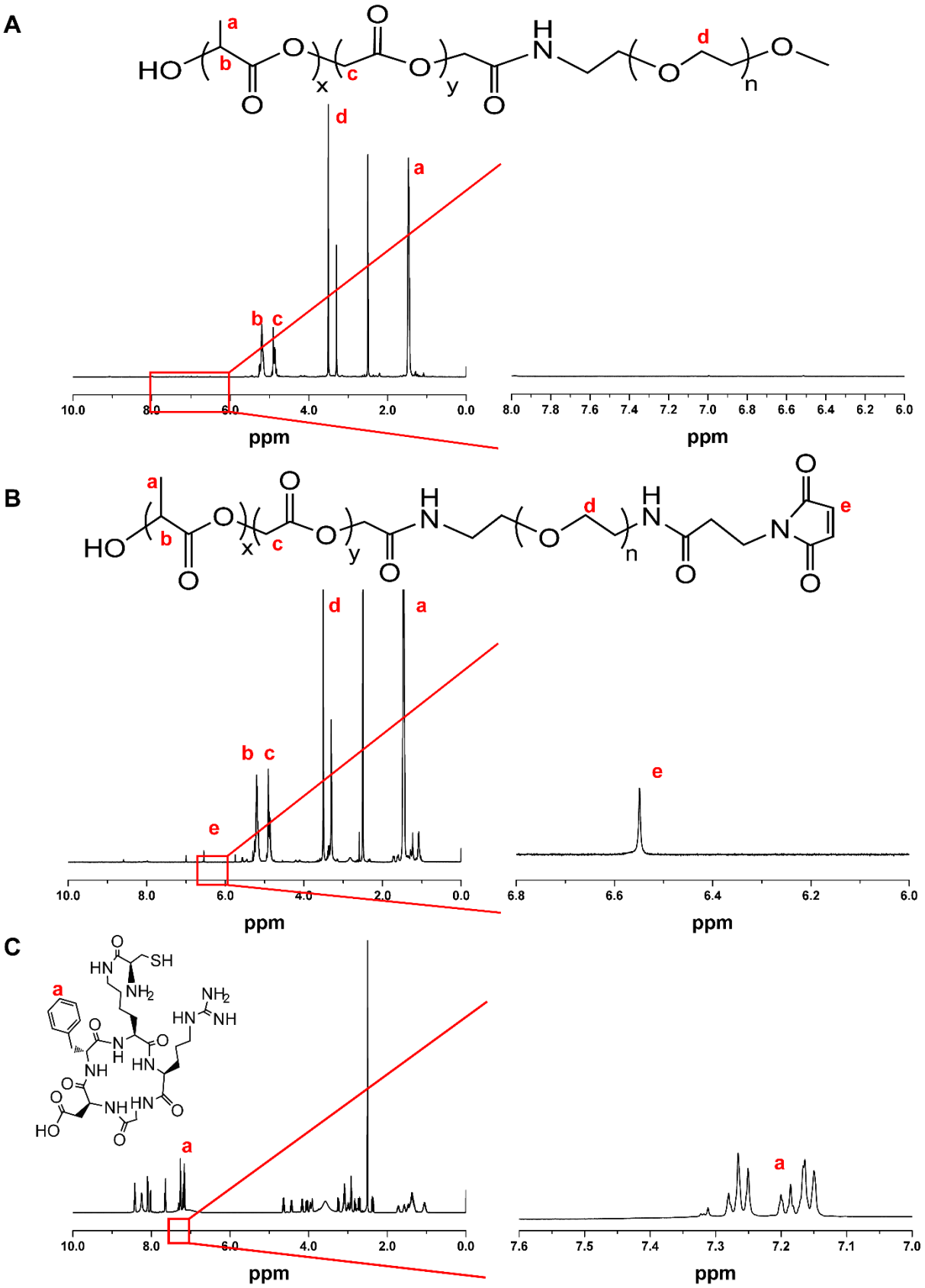

Figure S4. ^{1}H NMR spectra of PLGA$_{12k}$-mPEG$_{2k}$ **(A)**, PLGA$_{12k}$-PEG$_{2k}$-Mal **(B)** and c(RGDfKC) **(C)** in DMSO-d6. **(A)** PLGA$_{12k}$-mPEG$_{2k}$ was isolated in 91.1% (255 mg). The peaks in the ^{1}H NMR spectra at 1.46 and 5.21 ppm were assigned to the polylactide protons of PLGA, and the peaks at 4.85 ppm were assigned to polyglycolide protons of PLGA and the peak at 3.51 ppm corresponded to the PEG protons.

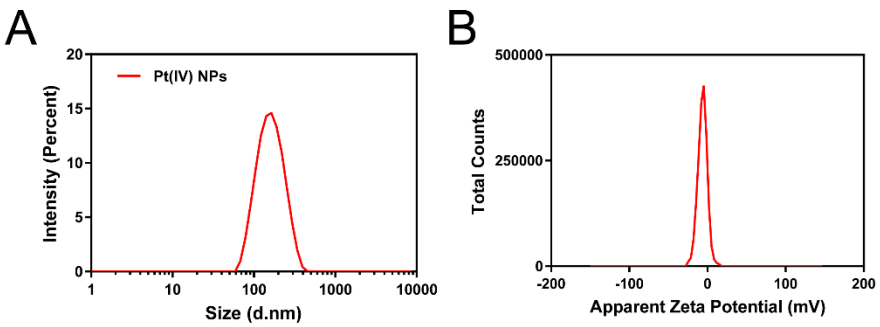

Figure S5. Size distribution **(A)** and Zeta potential **(B)** of Pt(IV) NPs.

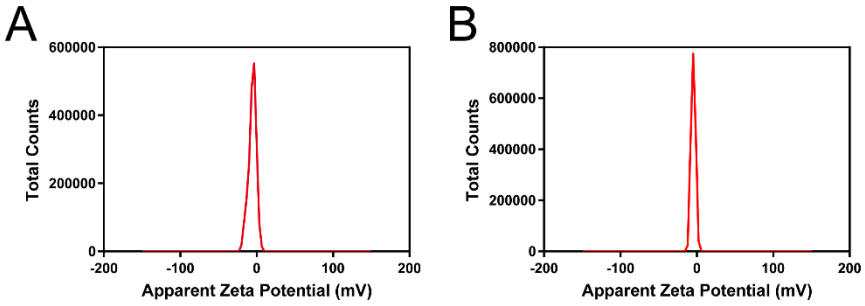

Figure S6. Zeta potential of Pt(IV) NP-cRGD before US exposure **(A)** and after US exposure **(B)**.

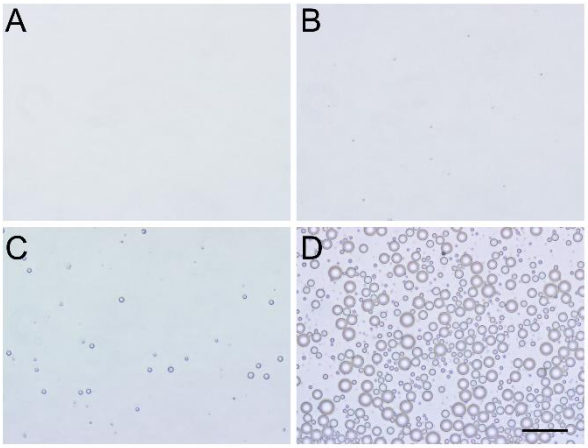

Figure S7. Microscopic images of the phase transition of Pt(IV) NP-cRGD at different temperatures. (A) 25 ºC; **(B)** 37 ºC; **(C)** 60 ºC; **(D)** 70 ºC. Original magnification, 100×; scale bar, 200 μm.

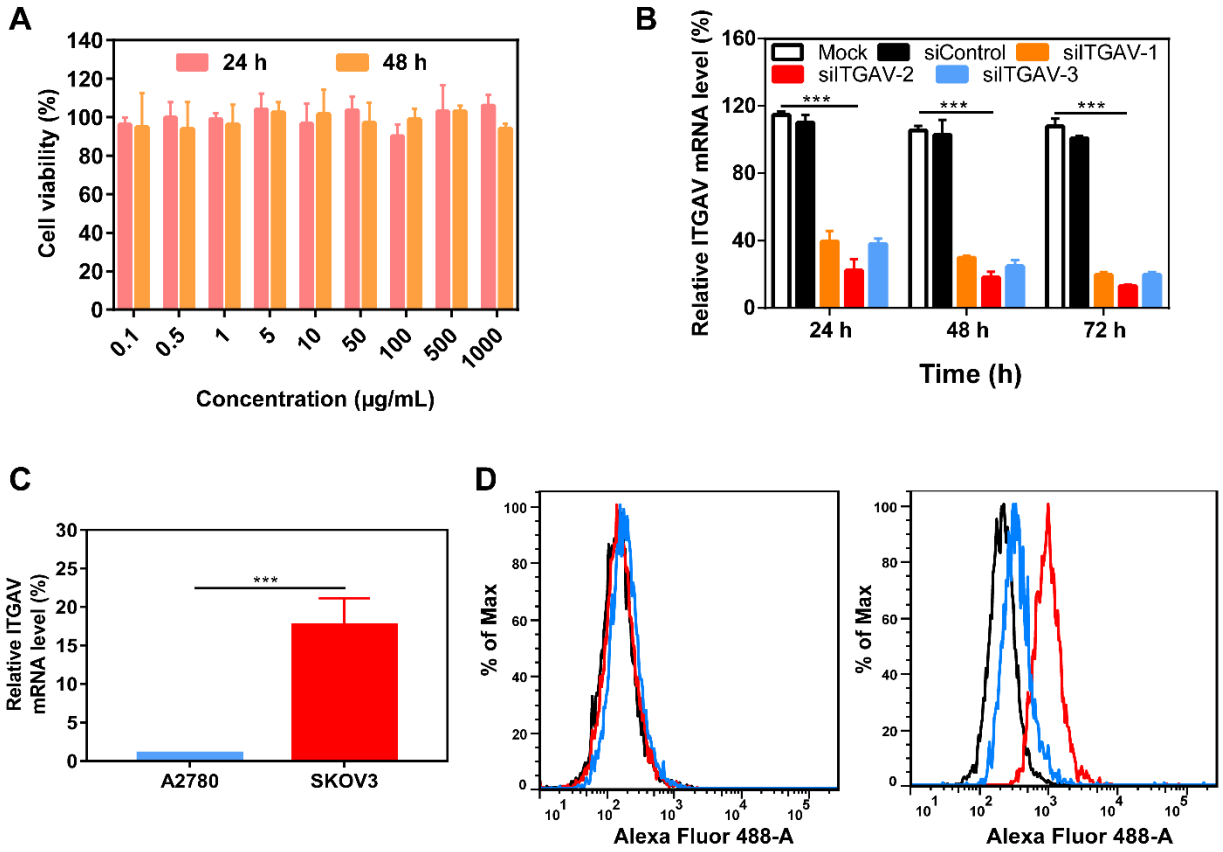

Figure S8. (A) Cell viability of SKOV3 cells with the treatment of various concentrations of cRGD for 24 h and 48 h. **(B)** The siRNA against integrin alpha V (si*ITGAV*) silencing effect in SKOV3 cells for 24 h, 48 h and 72 h. **(C)** Expression of alpha V mRNA in A2780 and SKOV3 cells. **(D)** Flow cytometric analysis of integrin expression of A2780 cells (left) and SKOV3 cells (right). Alexa Flour 488-labeled mouse IgG: control, black; Alexa Flour 488-labeled anti-$\alpha_v\beta_3$ integrin antibody: red; and Alexa Flour 488-labeled anti-$\alpha_v\beta_5$ integrin antibody: blue. The data are presented as the means ± SD of three independent experiments. Statistical significance in **(B)** was calculated by two-way ANOVA with Tukey's post hoc test. Statistical significance in **(C)** was calculated by Student's two-tailed *t*-test. $*P < 0.05$, $**P < 0.01$, $***P < 0.005$, NS indicates $P > 0.05$.

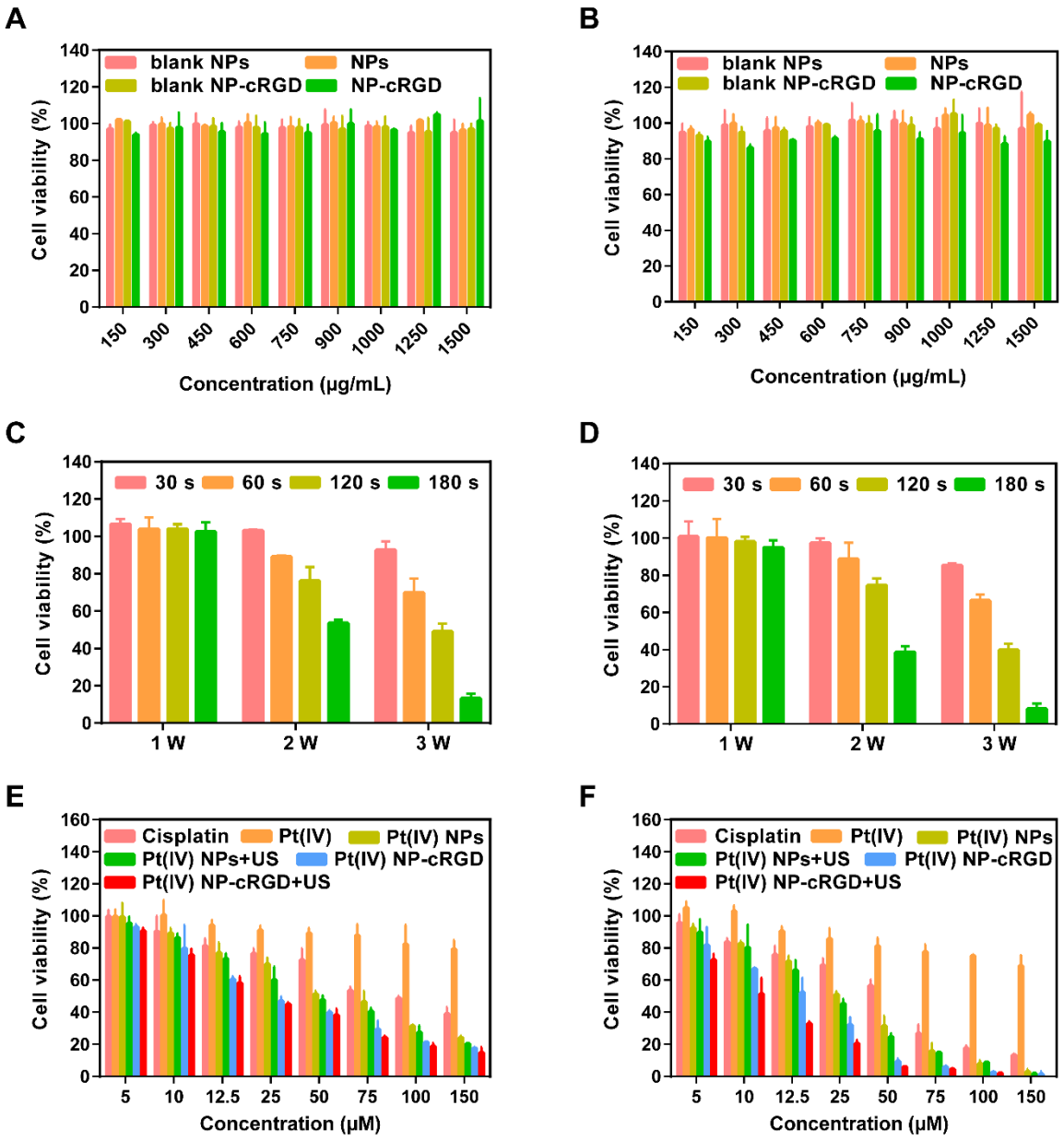

Figure S9. (A, B) Cell viability of SKOV3 cells with the treatment of various concentrations of blank NPs (Pt(IV) NPs without PFH and Pt(IV)), NPs (Pt(IV) NPs without Pt(IV)), blank NP-cRGD (Pt(IV) NP-cRGD without PFH and Pt(IV)) and NP-cRGD (Pt(IV) NP-cRGD without Pt(IV)) for 24 h **(A)** and 48 h **(B)**. **(C, D)** Cell viability of SKOV3 cells treated with different power and duration time of US for 24 h **(C)** and 48 h **(D)**. **(E, F)** Cell viability of SKOV3 cells with the treatment of various concentration of cisplatin, Pt(IV), Pt(IV) NPs, Pt(IV) NPs+US, Pt(IV) NP-cRGD and Pt(IV) NP-cRGD+US for 24 h **(E)** and 72 h **(F)**. The data are presented as the means ± SD of three independent experiments.

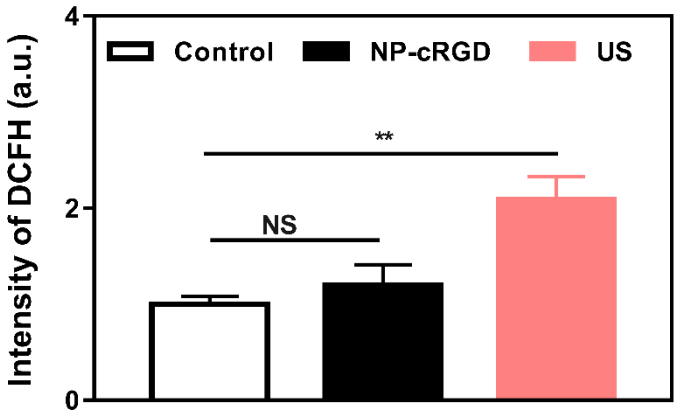

Figure S10. The ROS level using DCFH-DA dye with the treatment of NP-cRGD and US exposure for 48 h, detected by flow cytometry. The data are presented as the means ± SD of three independent experiments. Statistical significance was calculated by two-way ANOVA with Tukey's post hoc test. $*P < 0.05$, $**P < 0.01$, $***P < 0.005$, NS indicates $P > 0.05$.

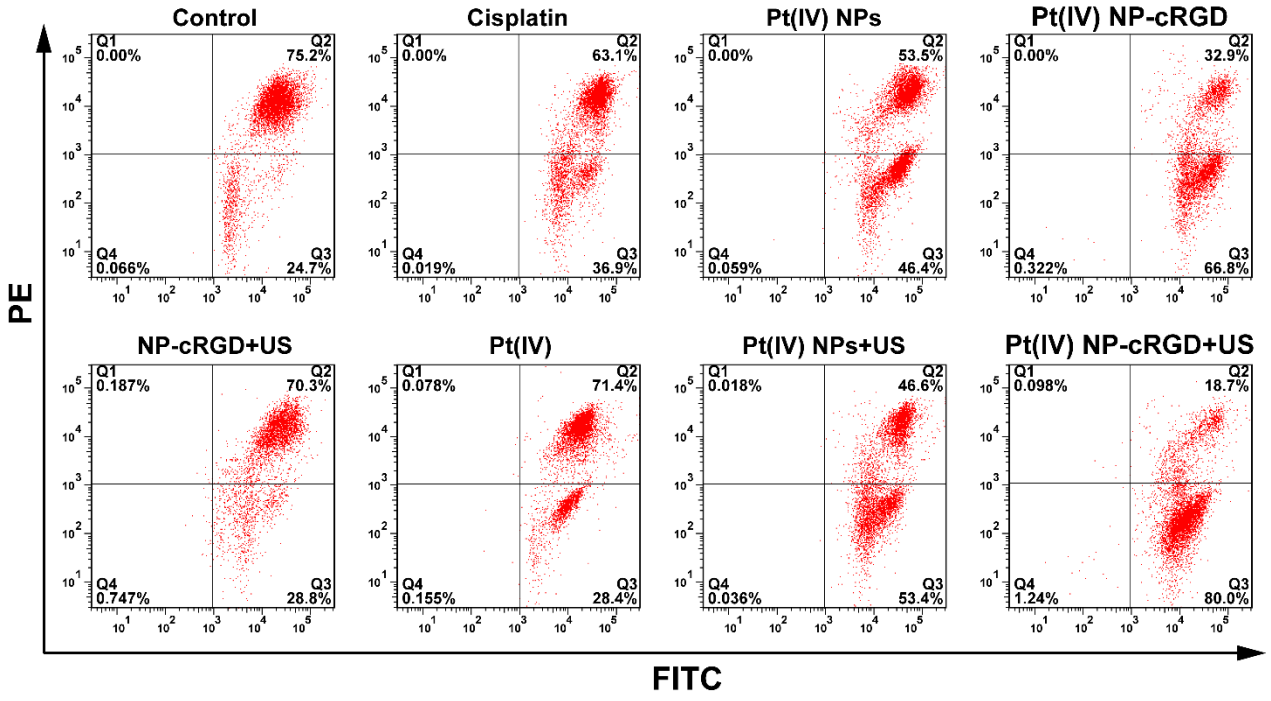

Figure S11. The flow cytometry analysis of the change in mitochondrial membrane potential ($\Delta\psi_m$) in cells with the treatment of NP-cRGD+US, cisplatin, Pt(IV), Pt(IV) NPs, Pt(IV) NPs+US, Pt(IV) NP-cRGD and Pt(IV) NP-cRGD+US (30 μM eq.) for 48 h. The data are presented as the means ± SD of three independent experiments.

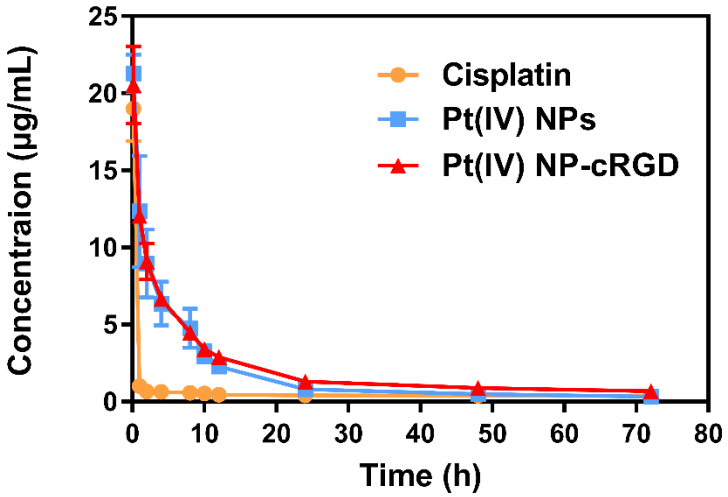

Figure S12. Pharmacokinetics of cisplatin, Pt(IV) NPs and Pt(IV) NP-cRGD after the intravenous injection (n = 6). The data are presented as the means ± SD.

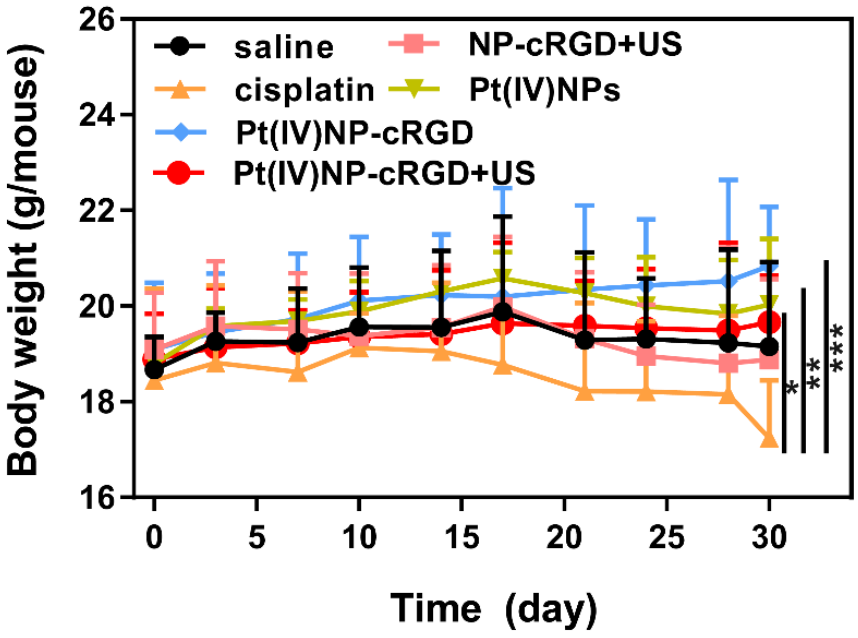

Figure S13. Body weight curves of tumor-bearing mice receiving different treatments (2.0 mg/kg platinum) (n = 6). The data are presented as the means ± SD. Statistical significance was calculated by two-way ANOVA with Sidak's post hoc test. *P < 0.05, **P < 0.01, ***P < 0.005, NS indicates P > 0.05.

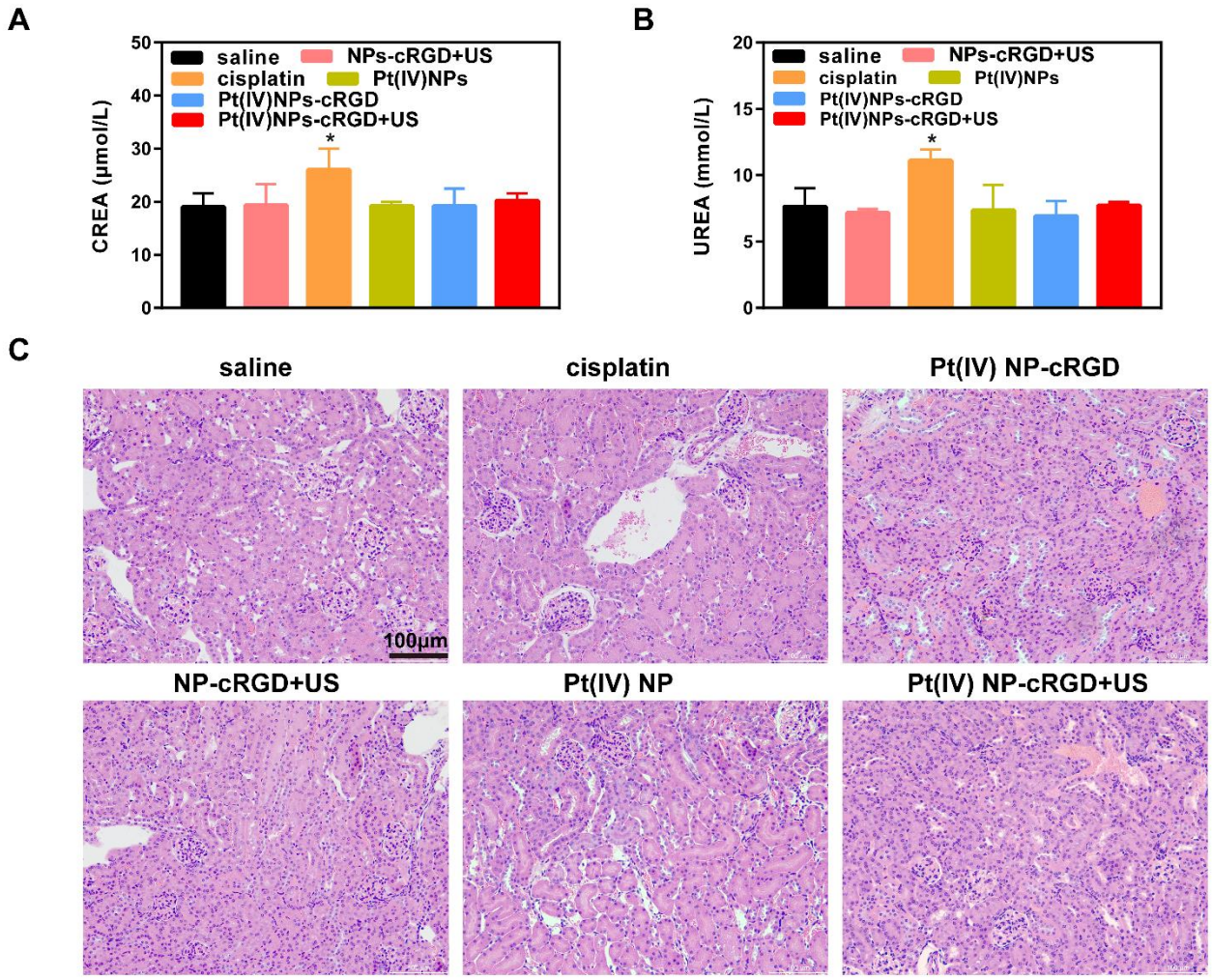

Figure S14. Pt(IV) NP-cRGD with US decreased nephrotoxicity. Serum CREA **(A)** and UREA **(B)** levels ($n = 6$). *$P < 0.05$, NS indicates $P > 0.05$ versus the saline group. **(C)** H&E staining of kidney sections in each group. All data are presented as the means ± SD. Statistical significance in **(A)** and **(B)** was calculated by one-way ANOVA with Tukey's post hoc test.

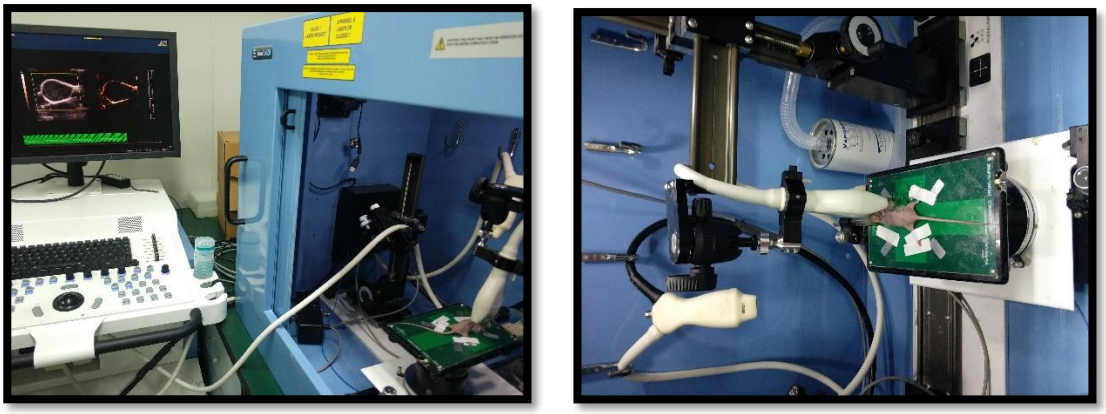

Figure S15. Images of *in vivo* US imaging of Pt(IV) NP-cRGD measuring in tumor-bearing nude mice by a VisualSonics 2100 imaging system with a MS-201 transducer.